# Supporting Information

# Flexible High-Energy Asymmetric Supercapacitors Based on MnO@C Composite Nanosheets Electrodes

Neng Yu,[‡a] Kai Guo,[‡b] Wei Zhang,[a] Xianfu Wang,[c*] and Ming-Qiang Zhu[a*]

[a.] Wuhan National Laboratory for Optoelectronics, Huazhong University of Science and Technology, Huazhong University of Science and Technology, Wuhan 430074, China

[b.] State Key Laboratory of Materials Processing and Die & Mould Technology, School of Materials Science and Engineering, Huazhong University of Science and Technology,Wuhan 430074, China

[c.] College of Physics, Optoelectronics and Energy, Suzhou key laboratory of advanced carbon materials and wearable energy technology & Collaborative Innovation Center of Suzhou Nano Science and Technology, Soochow University, Suzhou 215006, China

**Calculation methods**

**1. Single Electrode**

The specific capacitance ($C_s$) and areal capacitance ($C_a$) of the electrode is calculated from the galvanostatic charge-discharge curves by the following equations:

$C_s = It/m\Delta V$ (1)

$C_a = It/A\Delta V$ (2)

Where $I$ is the applied current (A), $t$ is the discharging time (s), $m$ is the mass of the active material (g), $A$ is the effective areal of the electrode and $\Delta V$ is the discharging potential window (V).

**2. ASC devices:**

The capacitance ($C$), specific capacitance ($C_S$) and areal capacitance ($C_A$) are calculated from the galvanostatic charge-discharge curves using the following equations:

$C = i/(-dV/dt)$ (3)

$C_S = C/S$ (4)

$C_A = C/A$ (5)

where $i$ is the applied current (A), $dV/dt$ is the slope of the discharge curve (V/s), $S$ is the total mass of the active material (g), $A$ is the areal of device ($cm^2$).

Energy density ($E$) and Power density ($P$) of the devices were obtained from the following equations:

$$E = \int_0^{\Delta t} IV(t)dt \quad (6)$$

$P = E/\Delta t$ (7)

Where $I$ is the discharging current, $V$ is the discharging voltage, $dt$ is the discharge time, and $\Delta t$ is the discharge time.

**3. Balance the charge of electrodes in asymmetric supercapacitors**

As for an ASC device, it is well-known that the charge balance can be following the relationship $Q_+ = Q_-$, where $Q_+$ is the charges stored at the positive and $Q_-$ is the charges stored at the negative electrodes .The charge storage by each electrode depends on the areal capacitance ($C_A$), the potential range for the charge/discharge process ($\Delta E$) and the effective areal of the electrode ($A$). The charge can be following equations:

$Q = C_A \times \Delta E \times A$

In order to obtain $Q_+ = Q_-$, the areal balance will be expressed as follows:

$$\frac{A_+}{A_-} = \frac{C_- \Delta E_-}{C_+ \Delta E_+} = 2:0.73$$

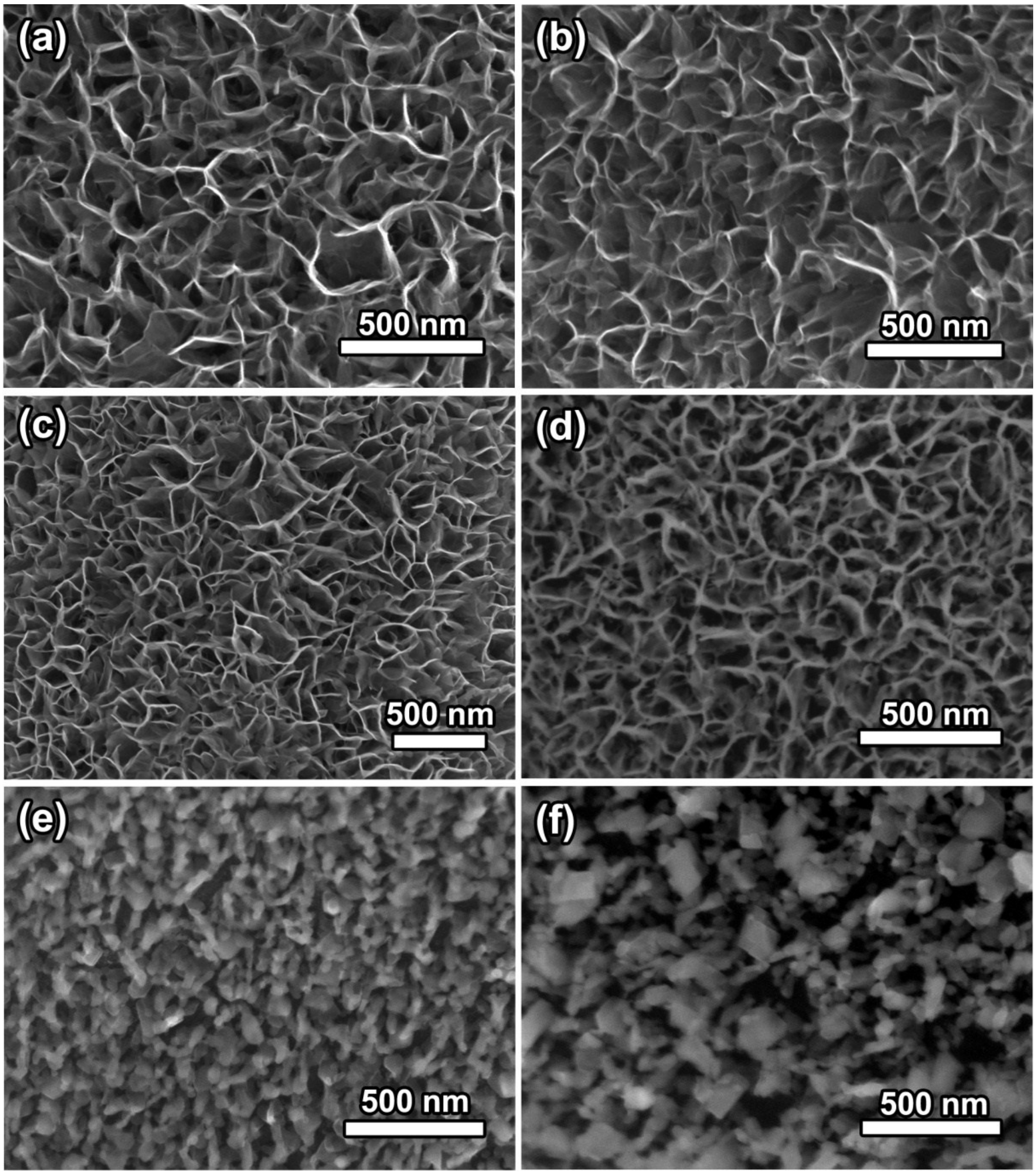


**Figure S1.** FESEM images of (a) pristine $MnO_2$/CFs and calcined products in $N_2$ at different temperatures named Mn/CFs-x, x = (b) 200 °C, (c) 300 °C, (d) 400 °C, (e) 500 °C, (f) 600 °C.

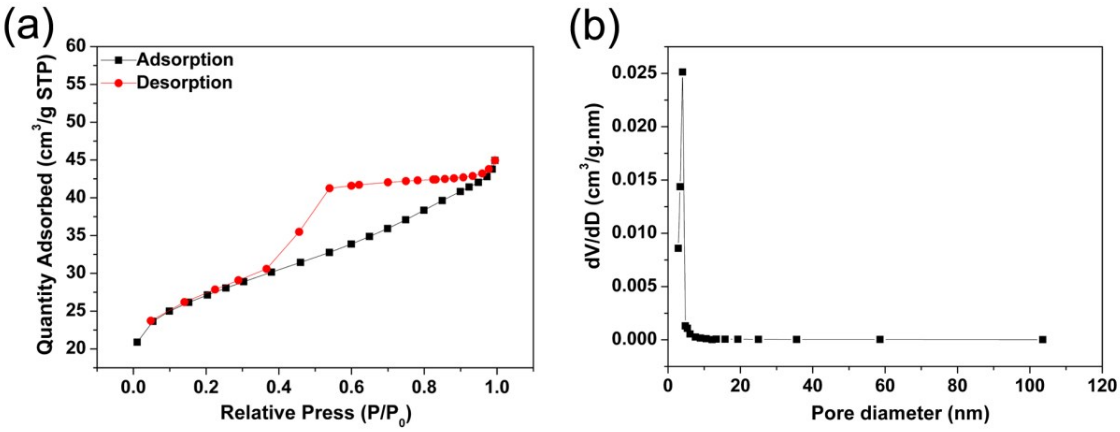


**Figure S2.** (a) Nitrogen adsorption-desorption isotherms, and (b) pore size distribution plot of MnO@C.

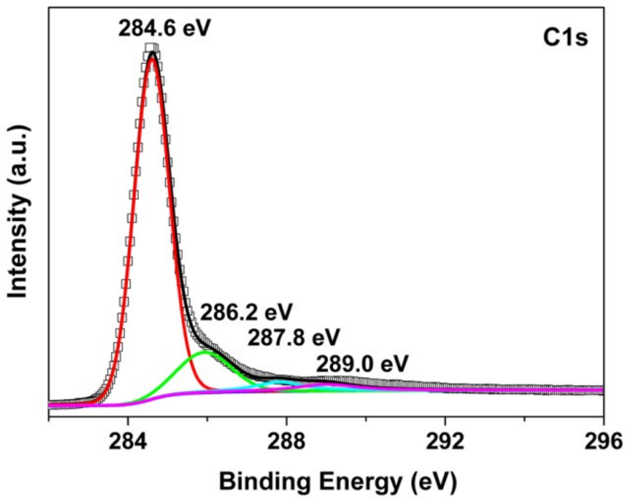


**Figure S3.** High-Resolution XPS C1s spectrum of MnO@C.

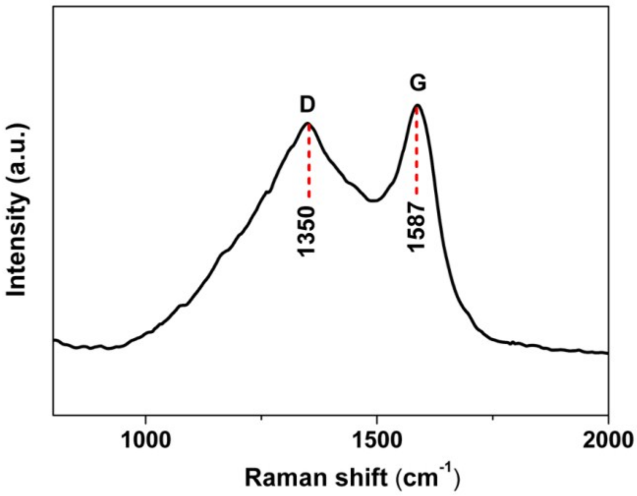


**Figure S4.** Raman spectrum of MnO@C composite.

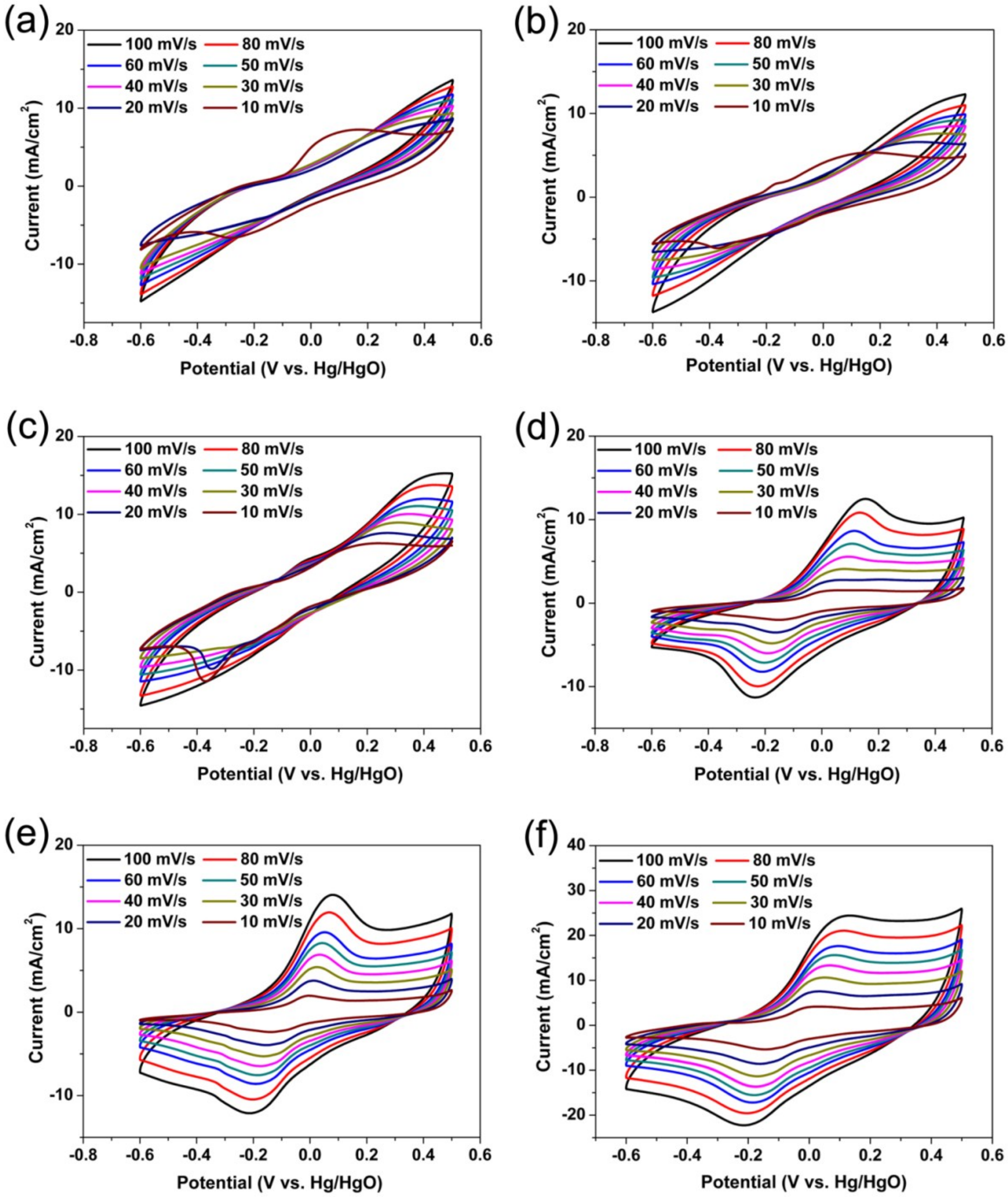


**Figure S5.** CV curves of (a) $MnO_2$/CFs and Mn/CFs-x, x = (b) 200 °C, (c) 300 °C, (d) 400 °C, (e) 500 °C, (f) 600 °C.

Table S1. Comparison of electrochemical performance for previous negative electrodes, other MnOx electrodes and MnO@C composite electrode in this paper.

| Electrode materials | Electrolyte | Potential range (V vs.Ag/AgCl, SCE or Hg/Hgo) | Specific capacitance (F/g) | Ref |
|---|---|---|---|---|
| $Fe_2O_3$ nanotubes | 5 M LiCl | -0.8 to 0 V | 257.8 F/g at 1.4 A/g | 1 |
| $V_2O_5$@PPy Nanoribbon | 0.5 M $K_2SO_4$ | -0.9 to 0.1 V | 308 F/g at 0.1 A/g | 2 |
| γ-FeOOH nanosheet | 1 M $Li_2SO_4$ | -0.8 to -0.1 V | 310.3 F/g at 0.13 A/g | 3 |
| Amorphous FeOOH QDs/FGS | 1 M $Li_2SO_4$ | -0.8 to 0 V | 365 F/g at 1 A/g | 4 |
| activated carbon nanofiber | 6 M KOH | -1.0 to 0 V | 455 F/g at 1mv/s | 5 |
| RGO/$MoO_3$ | 1 M $Na_2SO_4$ | -1.0 to 0 V | 291 F/g at 2 mV/s | 6 |
| carbon nanotube (CNT)-graphene foam | 1 M $Na_2SO_4$ | -0.8 to 0.2 V | 280.4 F/g at 1 A/g | 7 |
| $Bi_2O_3$/carbon nanofiber | 1 M $Na_2SO_4$ | -0.9 to 0 V | 51 F/g at 3 $mA/cm^2$ | 8 |
| $MnFe_2O_4$/graphene/polyaniline | 1 M NaCl | -0.55 to 0.25 V | 241 F/g at 0.5 $mA/cm^2$ | 9 |
| MnO@C/CC | 3M KOH | -0.6 to 0.5 V | 662.9 F/g, 716 $mF/cm^2$ at 4 $mA/cm^2$ | Our work |
| $WO_3$@PPy core-shell nanowire arrays | 3 M NaOH | -1.0 to 0 V | 253 $mF/cm^2$ at 0.67 $mA/cm^2$ | 10 |
| α-$Fe_2O_3$@PANI core-shell nanowire arrays | 1M $Na_2SO_4$ | -0.8 to 0 V | 103 $mF/cm^2$ at 0.86 $mA/cm^2$ | 11 |
| $Mn_3O_4$/ on conducting paper | 1.0 M NaOH | -0.8 to 0 V | 432 $mF/cm^2$ at 5 mV/s | 12 |
| N-$Fe_2O_3$ nanorods | 3 M LiCl | -0.8 to 0 V | 277.3 $mF/cm^2$ at 10 mV/s | 13 |
| sulphur-doped $Co_3O_4$ | 5 M LiCl | -0.8 to 0 V | 0.55 $F/cm^2$ at 10 mV/s | 14 |
| Three-Dimensional $CoSe_2$ | 1 M $Na_2SO_4$ | -0.8 to 0 V | 332 $mF/cm^2$ at 1 $mA/cm^2$ | 15 |
| $MnO_x$ NF | 0.5 M $Na_2SO_4$ | -0.2 to 0.8 V | 360.7 F/g at 1 A/g | 16 |
| $MnO_x$/CNFs | 0.5 M $Na_2SO_4$ | -0.2 to 0.8 V | 211 F/g at 0.25 A/g | 17 |
| MnOx-N-CS | 6 M KOH | -1.0 to 0 V | 258 F/g at 1 mV/s | 18 |
| $Mn_3O_4$@C nanowires | 1 M $Na_2SO_4$ | 0 to 0.8 V | 197 F/g at 2.5 mV/s | 19 |
| rGO/$Mn_3O_4$ | Saturate$Na_2SO_4$ | 0 to 0.8 V | 193 F/g at 50 mA/g | 20 |
| $Mn_3O_4$@GR | 6 M KOH | -0.6 V to 0.4 V | 250 F/g at 0.5 A/g | 21 |
| $Mn_3O_4$-GO | 0.5 M $Na_2SO_4$ | 0 to 1 V | 225 F/g at 5 mV/s | 22 |

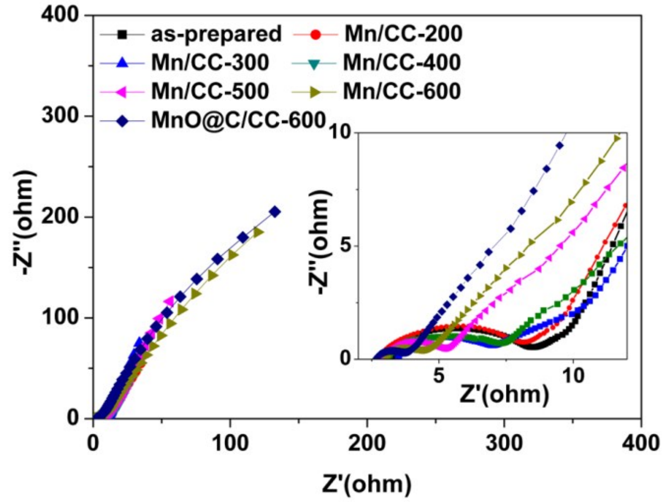


**Figure S6**. Nyquist plots of the MnO@C/CC electrode, Mn/CC-x electrode.

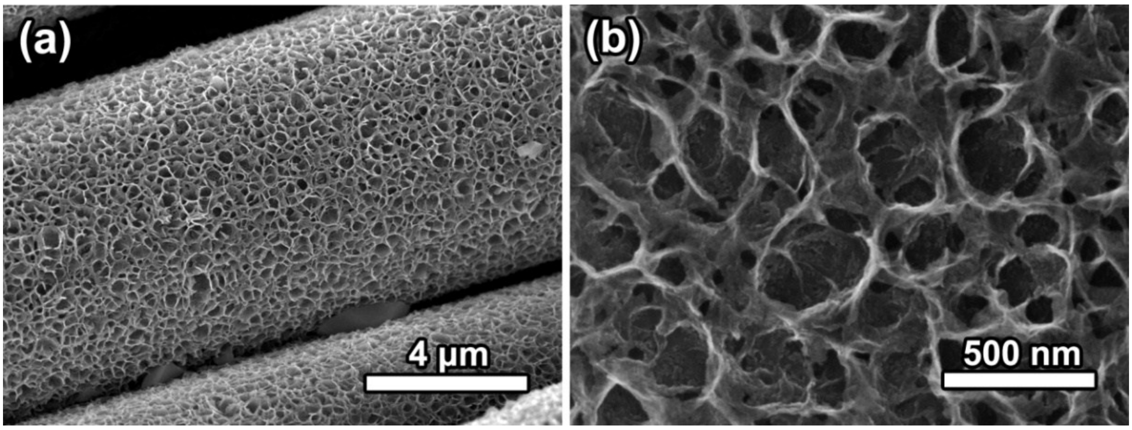


**Figure S7.** FESEM images of MnO@C/CFs after 5000 charge/discharge cycles at 10 $mA/cm^2$ in 3 M KOH solution.

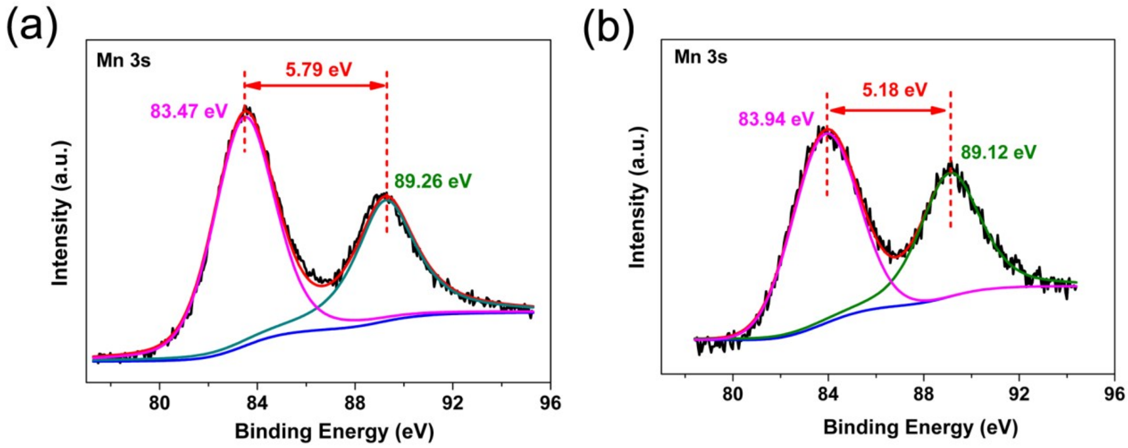


**Figure S8.** XPS spectra for MnO@C stripped off from CF cloth (a) before and (b) after 5000 charge/discharge cycles.

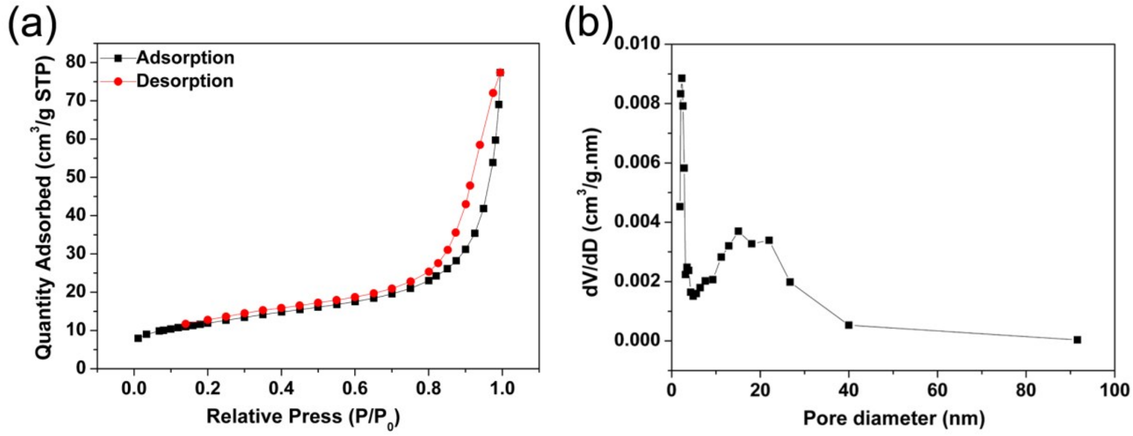


**Figure S9.** (a) Nitrogen adsorption-desorption isotherms, and (b) pore size distribution plot of $Co_3O_4$.

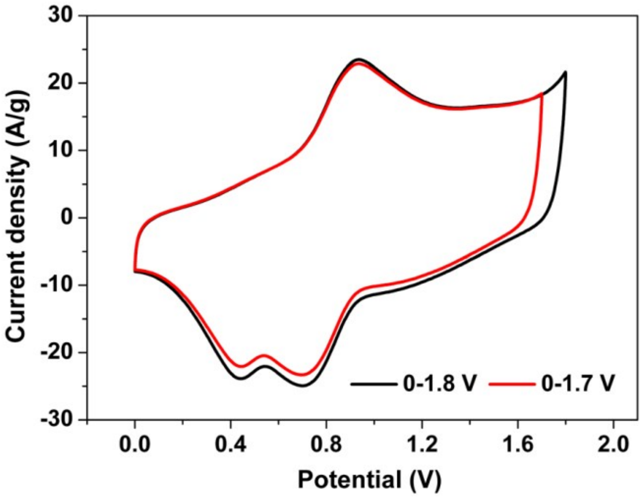


**Figure S10.** CV curves of ASCs at 100 mV/s in 3 M KOH.

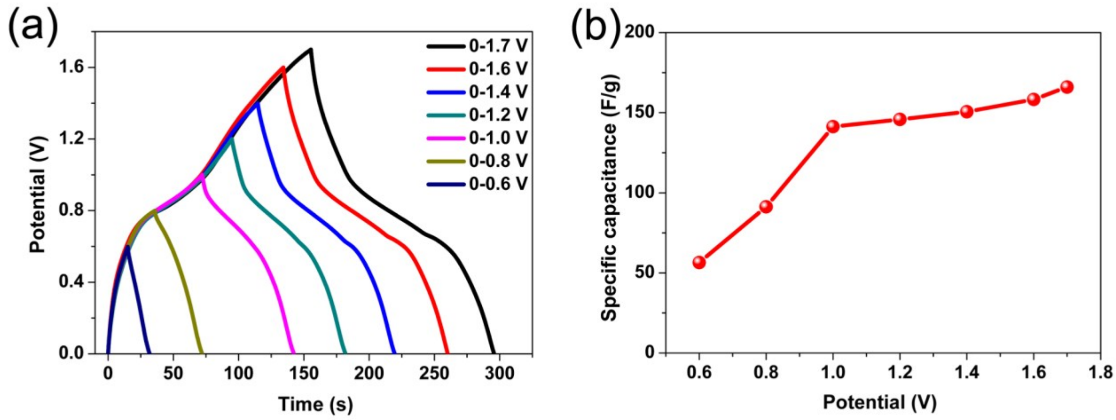


**Figure S11.** (a) Galvanostatic discharge/charge curves collected at different voltage windows. (b) Specific capacitance calculated from galvanostatic discharge/charge curves as a function of voltage window for the assembled ASC devices.

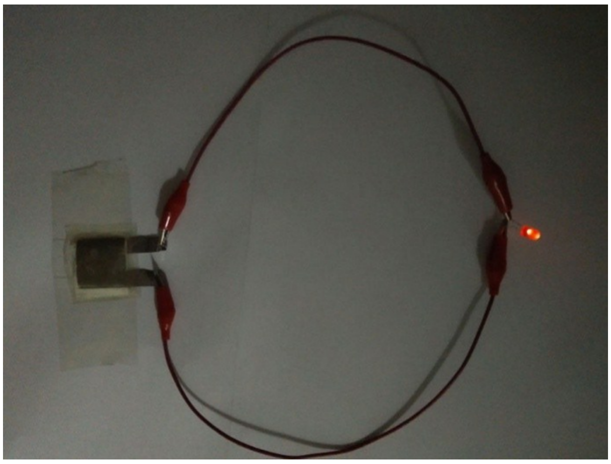

**Figure S12.** An LED indicator powered by the ASC device.

**References**


1. P. H. Yang, Y. Ding, Z. Y. Lin, Z. W. Chen, Y. Z. Li, P. F. Qiang, M. Ebrahimi, W. J. Mai, C. P. Wong, Z. L. Wang, *Nano Lett.*, 2014, **14**, 731-736.
2. Q. T. Qu, Y. S. Zhu, X. W. Gao, Y. P. Wu, *Adv. Energy Mater.*, 2012, **2**, 950-955.
3. Y. C. Chen, Y. G. Lin, Y. K. Hsu, S. C. Yen, K. H. Chen, L. C. Chen, *Small*, 2014, **10**, 3803-3810.
4. J. Q. Liu, M. b. Zheng, X. Q. Shi, H. B. Zeng, H. Xia, *Adv. Funct. Mater.*, 2016, **26**, 919-930.
5. Z. J. Fan, J. Yan, T. Wei, L. J. Zhi, G. Q. Ning, T. Y. Li, F. Wei, *Adv. Funct. Mater.*, 2011, **21**, 2366-2375.
6. J. Chang, M. H. Jin, F. Yao, T. H. Kim, V. T. Le, H. Y. Yue, F. Gunes, B. Li, A. Ghosh, S. S. Xie, Y. H. Lee, *Adv. Funct. Mater.*, 2013, **23**, 5074-5083.
7. Z. Y. Zhang, F. Xiao, L. H. Qian, J. W. Xiao, S. Wang, Y. Q. Liu, *Adv. Energy Mater.*, 2014, **4**, 867-872
8. H. H. Xu, X. L. Hu, H. L. Yang, Y. M. Sun, C. C. Hu, Y. H. Huang, *Adv. Energy Mater.*, 2014, **5**, 1401882.
9. K. V. Sankar, R. K. Selvan, *J. Power Sources*, 2015, **275**, 399-407.
10. F. M. Wang, X. Y. Zhan, Z. Z. Cheng, Z. X. Wang, Q. S. Wang, K. Xu, M. Safdar, J. He, *Small*, 2015, **11**, 749-755.
11. X. F. Lu, X. Y. Chen, W. Zhou, Y. X. Tong, G. R. Li, *ACS Appl. Mater. Interfaces*, 2015, **7**, 14843-14850.
12. J. X. Feng, S. H. Ye, X. F. Lu, Y. X. Tong, G. R. Li, *ACS Appl. Mater. Interfaces*, 2015, **7**, 11444-11451.
13. X. H. Lu, Y. X. Zeng, M. H. Yu, T. Zhai, C. L. Liang, S. L. Xie, M. S. Balogun, Y. X. Tong, *Adv. Mater.*, 2014, **26**, 3148-3155.
14. W. Xu, J. H. Chen, M. H. Yu, Y. X. Zeng, Y. B. Long, X. H. Lu, Y. X. Tong, *J. Mater. Chem. A*, 2016, **4**, 10779-10785.
15. N. Yu, M. Q. Zhu, D. Chen, *J. Mater. Chem. A*, 2015, **3**, 7910-7918.
16. E. Lee, T. Lee, B. Kim, *J. Power Sources*, 2014, **255**, 335-340.
17. Y. Yang, F. Yang, S. S. Lee, X. S. Li, H. R. Zhao, Y. Wang, S. J. Hao, X. Zhang, *Electrochimica Acta*, 2016, **191**, 1018-1025.
18. Y. X. Du, X. Zhao, Z. L. Huang, Y. Z. Li, Q. H. Zhang, *RSC Adv.*, 2014, **4**, 39087-39094.
19. K. B. Wang, X. Y. Ma, Z. Y. Zhang, M. B. Zheng, Z. Geng, Z. L. Wang, *Chem. Eur. J.*, 2013, **19**, 7084-7089.
20. Q. J. Ying, G. Feng, Z. Quan, W. Z. Yu, H. Han, L. B. Bei, W. W. Bo, W. X. Zhen, Q. J. Shan, *Nanoscale*, 2013, **5**, 2999-3005.
21. Y. H. Xiao, Y. B. Cao, Y. Y. Gong, A. Q. Zhang, J. H. Zhao, S. M. Fang, D. Z. Jia, F. Li, *J. Power Sources*, 2014, **246**, 926-933.
22. C. C. Zhang, L. G. Wang, Y. Z. Zhao, Y. Tian, J. B. Liang, *Carbon* , 2016, **107**, 100-108.
23. 